Title
Field emission from nanometer-scale tips of crystalline PbZrxTi1−xO3

Journal
Journal of Vacuum Science & Technology B Nanotechnology and Microelectronics Materials Processing Measurement and Phenomena, 31(2)

ISSN
2166-2746

Authors
Fletcher, Patrick C
Mangalam, Vengadesh Kumara R
Martin, Lane W
et al.

Publication Date
2013-03-01

DOI
10.1116/1.4793219

Peer reviewed

Field emission from nanometer-scale tips of crystalline $PbZr_xTi_{1-x}O_3$

Patrick C. Fletcher
Department of Mechanical Science and Engineering, University of Illinois at Urbana-Champaign, Urbana, Illinois 61801

Vengadesh Kumara R. Mangalam and Lane W. Martin
Department of Materials Science and Engineering and Materials Research Laboratory, University of Illinois at Urbana-Champaign, Urbana, Illinois 61801

William P. King[a)]
Department of Mechanical Science and Engineering, University of Illinois at Urbana-Champaign, Urbana, Illinois 61801 and Department of Materials Science and Engineering and Materials Research Laboratory, University of Illinois at Urbana-Champaign, Urbana, Illinois 61801

(Received 18 October 2012; accepted 4 February 2013; published 22 February 2013)

The authors report field emission from nanometer-sharp tips of polarized $PbZr_xTi_{1-x}O_3$ (PZT), silicon, and platinum. The PZT nanoemitters are fabricated in a batch fabrication process from single-crystal silicon tips that are coated with a 30 nm thick film of crystalline PZT. The nanoemitters start to emit electrons at fields as low as 2 V/μm and reach threshold emission, or turn-on, at fields as low as 3.9 V/μm. The turn-on field is 3.9 V/μm for $PbZr_{0.2}Ti_{0.8}O_3$, 6.8 V/μm for $PbZr_{0.52}Ti_{0.48}O_3$, and 10.75 V/μm for $PbZr_{0.8}Ti_{0.2}O_3$. The silicon nanoemitters have an electron emission turn-on field of 7.2 V/μm, and the platinum nanoemitters have an electron emission turn-on field of 5.75 V/μm. Using a Fowler-Nordheim analysis, the calculated effective work function of the $PbZr_{0.2}Ti_{0.8}O_3$ film is 1.00 eV, and the field amplification factor is ~1526. © *2013 American Vacuum Society*. [http://dx.doi.org/10.1116/1.4793219]

I. INTRODUCTION

Electron beams are used in a wide variety of commercial manufacturing processes, consumer products, and research tools, including free electron lasers,[1] x-ray tubes,[2] field emission displays,[3,4] and electron microscopes.[5,6] Electron field emission from cold cathodes using only large electric fields provides a compact, low-power, room temperature method for generating beams of electrons.[7–10] Much research has been published on reducing the electric field necessary to emit electrons from a surface.[11–17] Improved emitters requiring smaller electric fields would enable field emission in devices with portable, inexpensive power supplies. In general, however, microfabricated cathodes still require relatively large electric fields for cold cathode emission. This paper reports measurements of field emission from nanometer-scale tips of ferroelectric thin films, as well as silicon and platinum. These tips emit electrons at lower field strengths than other solid-state microfabricated cathodes that appear in the literature.

A cold cathode emits electrons when an electric field narrows the potential barrier, allowing electrons to tunnel from the cathode into vacuum.[7,18–20] This field emission process is enhanced by concentration of the electric field at sharp asperities[7,21,22] and reduction of the potential barrier with low work function cathode materials.[23–25] Emission current from a single emitting tip is limited by its nanometer-scale tip area, but the current can be increased by using many emitters in an array. The electron emission turn-on field, E_{ON}, can be defined as the electric field necessary to generate a current density of 0.5 μA/cm^2. Previous articles have reported silicon tip emitter arrays with turn-on electric fields of 13.3–70 V/μm (Refs. 26–28) and ferroelectric tip emitter arrays with turn-on electric fields of 4–19 V/μm.[13,29] The lowest reported turn-on field for a silicon tip coated with a ferroelectric film is 4 V/μm from $Ba_{0.67}Sr_{0.33}TiO_3$.[13] The reduced energy barrier to electron emission for ferroelectrics is not well understood from a theoretical standpoint, although the performance of a ferroelectric emitter has been observed to correlate with crystal quality and spontaneous polarization strength.[30,31] There is a lack of published data on field emission from microfabricated cathodes that use epitaxial PZT, and it is not known how PZT stoichiometry affects electron emission.

Cathode emitters based on carbon nanotubes (CNTs),[9] semiconductor nanowires,[17,32] and nanoparticles[14] have all demonstrated electron emission with low turn-on fields. In general, these nanomaterial-based cathodes have many individual emitters with random heights, nonuniform tip radii, and arbitrary locations. The height and radius of an emitter tip are critical parameters for controlling field emission behavior,[22] and accurate emitter placement may be important for device integration. In contrast to these bottom-up fabricated structures, batch-fabricated nanometer-scale tip emitters can have controlled spatial distribution and uniform tip morphology. Furthermore, circuit integration of field emitter devices requires batch microfabrication.

This paper presents field emission from nanometer-scale tips coated with various compositions of $PbZr_xTi_{1-x}O_3$ (PZT x:1 − x), silicon (Si) and platinum (Pt). The nanoemitters are batch microfabricated, and the crystalline PZT films are epitaxially grown directly on silicon, with no buffer layer. The ferroelectric nanoemitters have low turn-on electric fields and effective work functions compared to

a)Electronic mail: wpk@illinois.edu

published values for ferroelectric nanoemitters, and the devices demonstrate field enhancement factors comparable to or better than those of CNTs.

II. FABRICATION

Figure 1 shows an array of microfabricated tips 30 nm in radius and details of a single nanometer-scale tip of Si or PZT. Batch fabrication of sharp nanometer-scale silicon tips is described in detail elsewhere[33] and is briefly summarized here. The nanoemitters were fabricated on a 100 mm polished n-type silicon wafer 500 μm thick, doped with phosphorus to a dopant concentration near 1×10^{15} cm^{-3}. First, we formed pillars 2.7 μm in diameter and 2 μm tall using an inductively coupled plasma (ICP) deep reactive-ion etch (DRIE). An isotropic wet etch in HNA (2% hydrofluoric acid, 3% acetic acid, and 95% nitric acid) reduced the pillar terminus to 0.5 μm in diameter while maintaining a pillar base diameter of roughly 2.5 μm. Next, we used an iterative dry oxidation sharpening technique to sharpen the Si tips.[33] The tip dimensions were measured in a scanning electron microscope (SEM). The finished Si nanoemitters had a tip radius of about 10 nm, height of 1 μm, and base diameter of approximately 2 μm. The nanoemitters were arranged in a close-packed array with a 6 μm pitch, but with this fabrication method the pitch could be further reduced to about 3.5 μm. For later comparison, we sputter coated some nanoemitters with a 5 nm titanium (Ti) adhesion layer below a 75 nm Pt film, resulting in an average tip radius of about 60 nm across an emitter chip.

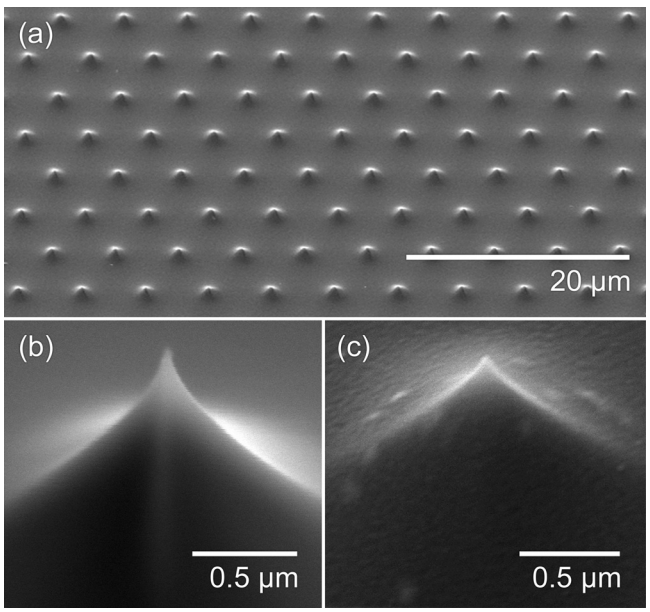

FIG. 1. SEM micrographs of a fabricated nanoemitter array. (a) The single-crystal silicon nanoemitters are batch fabricated in a 6 μm close-packed pitch with 3.2×10^6 emitters on a 10 mm $\times$ 10 mm chip. (b) The tips are fabricated through a combination of deep reactive-ion etching and oxidation sharpening. Before coating, the silicon tips are 1 μm tall, 2 μm wide at their base, and have an average tip radius of 10 nm. (c) After coating with a 30 nm thick epitaxial ferroelectric film, the tips have an average tip radius of 30 nm.

We deposited fully (00 *l*)-oriented thin films of ferroelectric PZT using pulsed-laser deposition. Prior to deposition, the native oxide on the Si nanoemitters was removed with a buffered oxide etch and less than 1 nm of native oxide grew during heating to the deposition temperature, according to oxide growth models using the chamber conditions. During deposition, the sample was maintained at 650 °C in 200 mTorr of oxygen while the laser fluence was 1.9 J/cm^2 and the laser repetition rate was 3 Hz. The final film was 30 nm thick, and the coated tips were about 30 nm in radius. The PZT film stoichiometries from PZT (80:20) to PZT (20:80) were selected to span the $PbZrO_3$–$PbTiO_3$ phase diagram and include PZT (52:48) near the morphotropic phase boundary.

The ferroelectric film quality of each stoichiometric composition was fully characterized. The films all had a similar root mean square roughness of 2–4 nm, measured by atomic force microscopy. The ferroelectric films were switched under an applied bias during piezoresponse force microscopy (PFM) analysis. The nonplanar morphology of the nanoemitters complicated some traditional characterization techniques. X-ray diffraction (XRD) on the nanoemitters with 30 nm thick PZT films was problematic; only the PZT (52:48) showed a strong 002 diffraction peak. For further verification, we grew similar PZT films that were 100 nm thick on flat Si wafers using identical growth conditions. Measurements of x-ray rocking curves confirmed that the flat films had similar crystal qualities. All three flat samples were fully (00 *l*)-oriented and the full-width-at-half-maximum dimensions of the 002 diffraction peaks were narrow and consistent. Both the flat and nonplanar films had no signature of secondary phases or other orientations. See Ref. 34 for further details on the PZT film quality including x-ray diffraction, atomic force microscopy, and piezoresponse force microscopy analysis. Overall, the films are of good quality and represent the first single-phase, (00 *l*)-oriented PZT films integrated on nanometer-scale tip arrays.

III. EXPERIMENT

Figure 2 shows the experimental setup for measuring field emission from the nanoemitter arrays. Emitters were tested

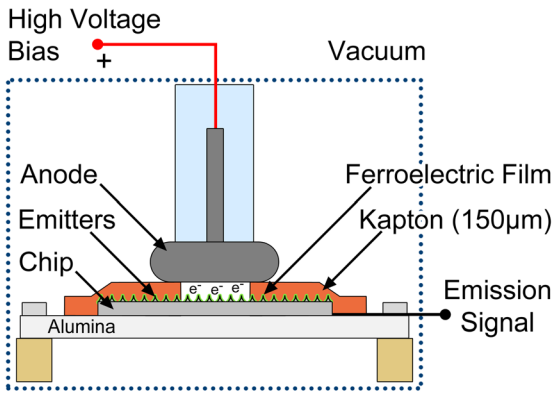

FIG. 2. (Color online) Field emission experimental setup. Samples are tested in vacuum at 10^{-6}–10^{-7} Torr. The anode has a high voltage positive bias, which generates a large electric field. The anode–cathode separation distance is 150 μm.

in a vacuum chamber at pressures between 10^{-6} and 10^{-7} Torr. Prior to emission studies, samples in the vacuum chamber were baked at 200 °C for 20 min to remove any residual water. A high voltage positive bias, V_M, on the machined stainless steel anode generated a macroscopic electric field, E_M, at the sample surface according to the emitter–anode separation. Kapton tape provided the macroscopic separation, d_M, of 150 μm between the anode and emitter chip. A 5.5 mm diameter hole in the center of the Kapton tape defined the macroscopic emission area, A_M, of 23.76 mm^2. The silicon chip was secured to the underlying alumina plate using cured silver paint, which also acted as an electrode for measuring macroscopic field emission current, I_M. We measured the emission current using this backside electrode connected in series to a 1 GΩ protection resistor, low-noise current amplifier, and low-noise preamplifier, in that order. The 1 GΩ resistor protected the instrumentation from high-voltage sparks, the low-noise current amplifier converted the emission current to a voltage signal, and the preamplifier low-pass filter removed 60 Hz noise. The combined gain from the current amplifier and preamplifier was 10^6.

During field emission measurements, the high voltage positive bias was increased in 100 V increments and 60 s time steps. The field emission current was characterized by two regimes. Above the emission turn-on field but below ~13 V/μm, the emission current was relatively noisy and fluctuated by approximately 0.1 μA at a given voltage bias. Above 13 V/μm, the current stabilized and was much less noisy with very little fluctuation. We measured emission current as a function of voltage bias at least four times for any given voltage and checked repeatability by measuring emission at random voltages. Measurement of the field emission current was repeatable and without hysteresis for both regimes.

IV. RESULTS AND DISCUSSION

Figure 3 shows measured field emission current, I_M, as a function of the macroscopic electric field, E_M. The current I_M represents the aggregate current from all operating tips in the array, and the field strength E_M is the voltage difference between anode and cathode divided by their separation distance, d_M. The reported current measurements are for the global, averaged emitter array rather than for individual tips, as it is unlikely that all tips were functional. The local current density and field strength likely vary with position on the three-dimensional cathode and are discussed later. Error bars show the standard deviation over at least four data sets. No electrons are emitted from the nanoemitters until E_M is sufficiently large to provide energy for the electrons to tunnel into vacuum. Thus, I_M is zero until E_M reaches some critical turn-on field, after which I_M increases with increasing E_M. This relationship is described by the Fowler-Nordheim (F-N) equation, discussed later. The Si and Pt emitters behave similarly, despite slightly different work functions: n-type Si with a phosphorus dopant concentration of 1×10^{15} cm^{-3} has a work function of 4.33 eV and polycrystalline Pt has a work function of 5.64 eV.[35,36] Interestingly, the PZT (52:48) and PZT (80:20) datasets also agree fairly well with each other above a field of 14 V/μm. Table I lists I_M at an arbitrary E_M threshold of 20 V/μm in order to compare each tip material. The maximum I_M for a given E_M increases with increasing Ti content in the PZT films.

TABLE I. Electron current and emission turn-on field for nanoemitters.

Tip material	Electron current[a] I_M (μA)	Emission turn-on field[b] E_{ON} (V/μm)
Si	1.98	7.2
Pt	1.83	5.8
PZT (20:80)	2.61	3.9
PZT (52:48)	1.50	6.8
PZT (80:20)	1.37	10.8

[a]The threshold electric field is 20 V/μm.
[b]The threshold current density is 0.5 $\mu A/cm^2$.

Figure 4 shows the measured macroscopic current density, J_M, as a function of E_M. J_M is calculated as I_M divided

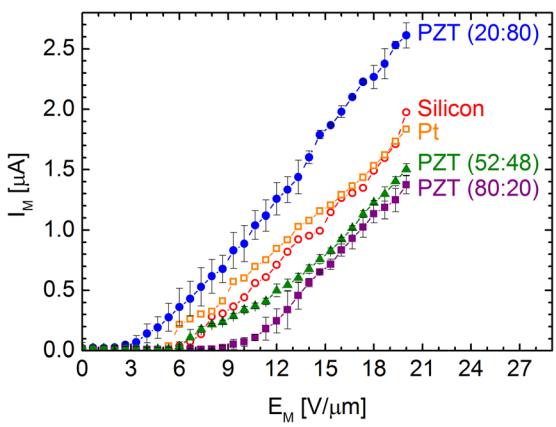

FIG. 3. (Color online) Measured field emission current. Error bars show the standard deviation from the mean of at least four data sets. Data are shown for silicon nanoemitters, platinum nanoemitters, and $PbZr_xTi_{1-x}O_3$ (PZT x:1−x) nanoemitters. For the PZT nanoemitters, emission turns on earlier and reaches higher emission currents with increasing titanium content.

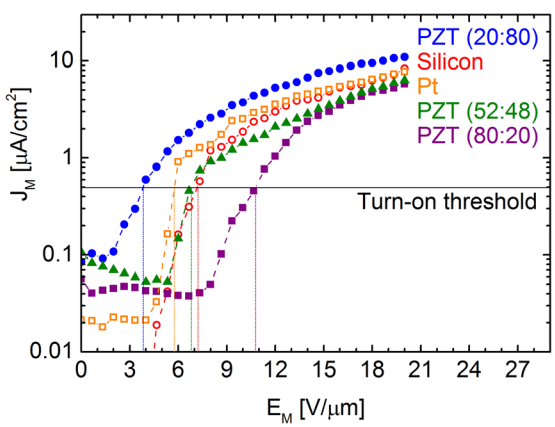

FIG. 4. (Color online) Measured field emission density. The electron emission turn-on field is defined as the electric field that generates a current density of 0.5 $\mu A/cm^2$, where the emission area is 23.8 mm^2. The nanoemitter turn-on field is 7.2 V/μm for silicon and 5.75 V/μm for platinum. The nanoemitter turn-on field is 3.9 V/μm for PZT (20:80), 6.8 V/μm for PZT (52:48), and 10.75 V/μm for PZT (80:20). The turn-on field decreases with increasing titanium content in the ferroelectric films.

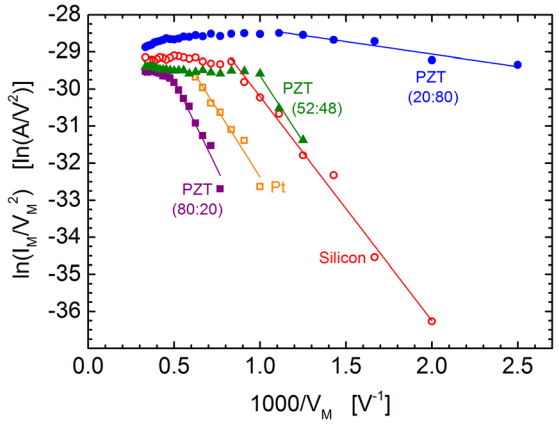

FIG. 5. (Color online) F-N type plots of measured emission data using the elementary F-N equation, $I_M = \alpha_M\ a\ A_M\ \phi^{-1}\ \gamma_C{}^2\ V_M{}^2\ d_M{}^{-2}\ \exp[-b\ \phi^{3/2}\ d_M/\gamma_C V_M]$. The F-N linear behavior after emission turn-on confirms field emission by electron tunneling into vacuum. Slopes of the linear fits are given in Table II and are used to calculate the effective work function, ϕ_{Eff}, the field enhancement factor, γ_C, and the area efficiency of emission, α_M.

by A_M. The electron emission turn-on field, E_{ON}, is listed for each tip material in Table I. The lowest E_{ON} is 3.9 V/μm for PZT (20:80). For comparison, batch fabricated silicon nanoemitters with similar microscopic morphology have turn-on fields of 13.3–70 V/μm.[26–28] Other researchers investigating field emission from dielectric- and ferroelectric-coated silicon tips report turn-on fields of 17 V/μm for $SrTiO_3$ (Ref. 27) and 19 V/μm for $Ba_xSr_{1-x}TiO_3$.[29] E_{ON} decreases with increasing Ti content in the PZT films, again suggesting that PZT stoichiometries with more Ti content are better field electron emitters. This observation is somewhat unexpected as the work function of PZT does not change considerably across the range of tested compositions. Rather, the large differences in E_{ON} likely arise from a different mechanism.

Figure 5 shows F-N type plots of the measured field emission data from Figs. 3 and 4. The technically complete F-N equation for large-area field emitters (LAFEs) is

$$I_M = \alpha_M \lambda_C a A_M \phi^{-1} \gamma_C{}^2 V_M{}^2 d_M{}^{-2} \exp[-v_F b \phi^{3/2} d_M/\gamma_C V_M], \quad (1)$$

where α_M is the area efficiency of emission, λ_C and v_F are correction factors, $a = 1.541434 \times 10^{-6}$ A eV V^{-2} and $b = 6.830890 \times 10^9$ $eV^{-3/2}$ V m^{-1} are universal F-N constants, ϕ is the emitter work function, and γ_C is the macroscopic field enhancement factor.[18,19,37] Assuming that λ_C and v_F are equal to unity, Eq. (1) reduces to an elementary F-N equation

$$I_M = \alpha_M a A_M \phi^{-1} \gamma_C{}^2 V_M{}^2 d_M{}^{-2} \exp[-b\phi^{3/2} d_M/\gamma_C V_M]. \quad (2)$$

We acknowledge that this F-N equation is simplified and does not rigorously account for λ_C and v_F. This approach, however, is widely used and allows us to make comparisons with literature values.[38] In Fig. 5, there is a linear relationship between $\ln(I_M/V_M{}^2)$ and $1000/V_M$ for data above the turn-on electric field, which confirms field emission by electron tunneling into vacuum. At relatively high electric fields, the F-N curves deviate to a secondary linear regime. The literature suggests that this deviation in LAFE F-N curve behavior is caused by secondary emission from alternative emission sites,[15,17,39] defects in the emitting film,[39] localized electronic states,[12] or interactions between emission sites in emitter arrays.[12]

The linear fit F-N slopes (FNSL) and intercepts (FNINT) are given in Table II and are used to calculate field emission metrics. Using Eq. (2), the effective work function of a nanoemitter is

$$\phi_{\text{Eff}} = \phi_{\text{Si}} (\text{FNSL}_{\text{film}}/\text{FNSL}_{\text{Si}})^{2/3}, \quad (3)$$

where ϕ_{Si} is the Si nanotip work function, $\text{FNSL}_{\text{film}}$ is the linear fit F-N slope of the material of interest, and FNSL_{Si} is the F-N slope of the Si nanoemitters. This equation is valid with the assumptions that the Si nanoemitter work function is 4.33 eV and that all the nanoemitters have identical field enhancement factors. Again using Eq. (2), the geometric field enhancement factor for all the nanoemitters is

$$\gamma_C = (-b\phi^{3/2} d_M)/(\text{FNSL} \times 10^3), \quad (4)$$

where the FNSL is in units reported by Table II. From Eq. (2), the area efficiency of emission is

$$\alpha_M = a^{-1} \gamma_C{}^{-2} A_M{}^{-1} \phi d_M{}^2 \exp(\text{FNINT}). \quad (5)$$

The calculated effective work functions, field enhancement factors, and area efficiencies of emission are listed in Table II.

TABLE II. Emitter characteristics from Fowler-Nordheim analysis.

Tip material	FNSL ($\ln(A/V^2)\cdot V/1000$)	FNINT ($\ln(A/V^2)$)	Effective work function[a] ϕ_{Eff} (eV)	Field enhancement factor[b] γ_C	Area efficiency of emission[c] α_M
Si	−6.05	−24.15	4.33[d]	1526.0	3.712×10^{-14}
Pt	−7.29	−25.08	4.90	1526.0	1.658×10^{-14}
PZT (20:80)	−0.67	−27.72	1.00	1526.0	2.410×10^{-16}
PZT (52:48)	−7.14	−22.49	4.84	1526.0	2.180×10^{-13}
PZT (80:20)	−9.5	−25.02	5.85	1526.0	2.101×10^{-14}

[a] $\phi_{\text{Eff}} = \phi_{\text{Si}} \times (\text{FNSL}_{\text{film}}/\text{FNSL}_{\text{Si}})^{2/3}$, $\phi_{\text{Si}} = 4.33$ eV.
[b] $\gamma_C = (-6.83089 \times 10^9\ \text{V eV}^{-3/2}\ \text{m}^{-1} \times \phi^{3/2} \times d_M)/(\text{FNSL} \times 10^3)$.
[c] $\alpha_M = (1.541434 \times 10^{-6}\ \text{A eV V}^{-2})^{-1}\ \gamma_C{}^{-2}\ A_M{}^{-1}\ \phi\ \exp(\text{FNINT})\ d_M{}^2$.
[d] Reference 35.

The effective work function calculated from field emission F-N plots is a relative metric typically used to compare the performance of field emitters. A lower effective work function implies that there is a lower energy barrier preventing electrons from tunneling into vacuum, and these materials have lower electron emission turn-on fields. The calculated effective work functions, besides the Si value from the literature, do not agree with traditionally measured electron work function values from a source such as the *Handbook of Chemistry and Physics*.[36] The PZT (20:80) nanoemitters demonstrate the lowest effective work function for ferroelectric-coated Si reported to date. The PZT (20:80) tips have a mean effective work function of 1.00 eV, which is more than four times lower than the work function of the bare silicon tips. Low threshold electron emission correlates with well-developed perovskite grains.[29,40] PFM analysis and XRD rocking curves confirm that the PZT film is of high-quality despite growth directly on single-crystal Si with no buffer layer.

Because all the nanoemitters have about the same height and tip sharpness, γ_C is calculated to be about 1526, a large improvement over a planar surface of the same material without nanoemitters. This value compares favorably with γ_C of 300–1900 reported in the literature for carbon nanotube (CNT) field emitters,[9,11,39] which are considered superior field emitters. We attribute this large γ_C to the uniform tip morphology, uniform emitter spacing, and 10–30 nm radius of the nanometer-sharp tips. Importantly, the PZT nanoemitter spatial distribution, tip height, and tip radius are controlled during microfabrication. This is in contrast to CNTs, nanowires, and nanoparticles, which usually have a random distribution on a substrate with poorly controlled tip radii and emitter heights.

While the mechanism enhancing field emission from ferroelectric nanotips is not clear, we can identify some aspects of the underlying physics based on current and previous work. It is likely that there are many variables impacting electron ejection from these complex materials into vacuum. Indeed, published articles have suggested that field emission can be affected by electron affinity,[13] stoichiometric composition,[29] internal polarization strength,[30] interface structure,[31] and ferroelectric grain structure.[40] Emitters in the present work are unique because the ferroelectric films have nanometer-scale roughness and varying ratios of Zr to Ti atoms. From our experimental results of enhanced emission from these films, we hypothesize that the surface grain structure and/or the magnitude of the spontaneous polarization strength could be responsible for the observed variations in field emission. Nanometer-scale asperities determined by the average crystallite size and the average surface roughness may act as local emission sites, further concentrating the electric field and increasing global emission. Alternatively, the inherent electronic structure of ferroelectrics may result in an electronic field enhancement factor that does not occur for nonpolarized materials. The remnant polarization of PZT decreases with increasing Zr content,[41,42] and our observed trend for field emission has a direct correlation to Zr content. It is clear that future work should endeavor to isolate the critical factors affecting ferroelectric emission so that these films can be further optimized for electron beam generation.

V. CONCLUSIONS

In conclusion, we have measured field emission from silicon nanoemitters coated with three stoichiometric variations of ferroelectric $PbZr_xTi_{1-x}O_3$. These nanoemitters are fabricated using batch microfabrication processes for precise control over tip location and morphology. The crystalline PZT films are epitaxially grown directly on silicon, with no buffer layer, and demonstrate good perovskite crystallinity and polarization. The PZT (20:80) nanoemitter turn-on electric field of 3.9 V/μm and effective work function of 1.00 eV are lower than values previously reported for ferroelectric nanoemitters. From Fowler-Nordheim analysis, the nanoemitter field enhancement factor of $\sim$1526 is large even compared to carbon nanotube emitters. These nanometer-scale electron sources could be used in miniature x-ray sources or low-cost field emission displays.

ACKNOWLEDGMENTS

This work was supported by the DARPA AXIS program under Grant No. N66001-11-1-4195. Portions of this work were performed in the Materials Research Laboratory Central Facilities, University of Illinois.

[1]D. A. G. Deacon, L. R. Elias, J. M. J. Madey, G. J. Ramian, H. A. Schwettman, and T. I. Smith, Phys. Rev. Lett. **38**, 892 (1977).
[2]W. Coolidge, U.S. patent 1,211,092 (2 January 1917).
[3]Q. H. Wang, A. A. Setlur, J. M. Lauerhaas, J. Y. Dai, E. W. Seelig, and R. P. H. Chang, Appl. Phys. Lett. **72**, 2912 (1998).
[4]W. B. Choi *et al.*, Appl. Phys. Lett. **75**, 3129 (1999).
[5]V. K. Zworykin, Sci. Am. **167**, 111 (1942).
[6]K. C. A. Smith and C. W. Oatley, Br. J. Appl. Phys. **6**, 391 (1955).
[7]W. P. Dyke and W. W. Dolan, *Advances in Electronics and Electron Physics*, edited by L. Marton (Academic, New York, 1956), Vol. 8, p. 89.
[8]O. Auciello, M. Ray, D. Palmer, J. Duarte, G. McGuire, and D. Temple, Appl. Phys. Lett. **66**, 2183 (1995).
[9]W. A. de Heer, A. Châtelain, and D. Ugarte, Science **270**, 1179 (1995).
[10]C. A. Spindt, I. Brodie, L. Humphrey, and E. R. Westerberg, J. Appl. Phys. **47**, 5248 (1976).
[11]D. N. Davydov, P. A. Sattari, D. AlMawlawi, A. Osika, T. L. Haslett, and M. Moskovits, J. Appl. Phys. **86**, 3983 (1999).
[12]J. Yu, E. G. Wang, and X. D. Bai, Appl. Phys. Lett. **78**, 2226 (2001).
[13]W. P. Kang, A. Wisitsora-at, J. L. Davidson, O. K. Tan, W. G. Zhu, Q. Li, and J. F. Xu, J. Vac. Sci. Technol. B **19**, 1073 (2001).
[14]S. K. Marathe, P. M. Koinkar, S. S. Ashtaputre, M. A. More, S. W. Gosavi, D. S. Joag, and S. K. Kulkarni, Nanotechnology **17**, 1932 (2006).
[15]N. Perea-Lopez *et al.*, ACS Nano **5**, 5072 (2011).
[16]D. Ye, S. Moussa, J. D. Ferguson, A. A. Baski, and M. S. El-Shall, Nano Lett. **12**, 1265 (2012).
[17]W.-D. Zhu, C.-W. Wang, J.-B. Chen, D.-S. Li, F. Zhou, and H.-L. Zhang, Nanotechnology **23**, 455204 (2012).
[18]R. H. Fowler and L. Nordheim, Proc. R. Soc. London, Ser. A **119**, 173 (1928).
[19]E. L. Murphy and R. H. Good, Jr., Phys. Rev. **102**, 1464 (1956).
[20]G. Rosenman, D. Shur, Y. E. Krasik, and A. Dunaevsky, J. Appl. Phys. **88**, 6109 (2000).
[21]R. G. Forbes, C. J. Edgcombe, and U. Valdre, Ultramicroscopy **95**, 57 (2003).
[22]E. G. Pogorelov, Y.-C. Chang, A. I. Zhbanov, and Y.-G. Lee, J. Appl. Phys. **108**, 044502 (2010).
[23]O. Auciello, J. C. Tucek, A. R. Krauss, D. M. Gruen, N. Moldovan, and D. C. Mancini, J. Vac. Sci. Technol. B **19**, 877 (2001).

[24]F. Jin, Y. Liu, C. M. Day, and S. A. Little, J. Vac. Sci. Technol. B **25**, 1785 (2007).
[25]J. B. You, X. W. Zhang, P. F. Cai, J. J. Dong, Y. Gao, Z. G. Yin, N. F. Chen, R. Z. Wang, and H. Yan, Appl. Phys. Lett. **94**, 262105 (2009).
[26]C. T. Sune, G. W. Jones, and D. Vellenga, J. Vac. Sci. Technol. B **10**, 2984 (1992).
[27]H. J. Bian, X. F. Chen, J. S. Pan, C. Q. Sun, and W. Zhu, J. Vac. Sci. Technol. B **25**, 817 (2007).
[28]Y. Gurbuz, W. P. Kang, J. L. Davidson, O. K. Tan, W. G. Zhu, Q. Li, and J. F. Xu, J. Vac. Sci. Technol. B **25**, 1560 (2007).
[29]X. F. Chen, W. Zhu, H. Lu, J. S. Pan, H. J. Bian, O. K. Tan, and C. Q. Sun, Ceram. Int. **34**, 971 (2008).
[30]H. Lu, J. Pan, X. Chen, and W. Zhu, J. Appl. Phys. **102**, 014113 (2007).
[31]X. F. Chen, H. Lu, W. G. Zhu, and O. K. Tan, Surf. Coat. Tech. **198**, 266 (2005).
[32]D. Banerjee, S. H. Jo, and Z. F. Ren, Adv. Mater. **16**, 2028 (2004).
[33]R. B. Marcus, T. S. Ravi, T. Gmitter, K. Chin, D. Liu, W. J. Orvis, D. R. Ciarlo, C. E. Hunt, and J. Trujillo, Appl. Phys. Lett. **56**, 236 (1990).
[34]See supplementary material at http://dx.doi.org/10.1116/1.4793219 for further details on the PZT film quality including x-ray diffraction, atomic force microscopy, and piezoresponse force microscopy analysis.
[35]A. Novikov, Solid State Electron. **54**, 8 (2010).
[36]W. M. Haynes, *CRC Handbook of Chemistry and Physics* (CRC, Boca Raton, FL, 2012).
[37]K. L. Jensen, *Advances in Imaging and Electron Physics*, edited by L. J. Kevin (Elsevier, Amsterdam, 2007), Vol. 149, p. 1.
[38]R. G. Forbes, Nanotechnology **23**, 095706 (2012).
[39]H. Gao *et al.*, J. Appl. Phys. **93**, 5602 (2003).
[40]W. P. Kang, A. Wisitsora-at, J. L. Davidson, O. K. Tan, W. G. Zhu, Q. Li, and J. F. Xu, J. Vac. Sci. Technol. B **21**, 453 (2003).
[41]S. H. Kim *et al.*, Jpn. J. Appl. Phys. 1 **42**, 5952 (2003).
[42]C. M. Foster, G. R. Bai, R. Csencsits, J. Vetrone, R. Jammy, L. A. Wills, E. Carr, and J. Amano, J. Appl. Phys. **81**, 2349 (1997).